



Enhanced direct deoxygenation of anisole to benzene on SiO₂-supported Ni-Ga alloy and intermetallic compound

Ying Zheng, Ning Zhao, Jixiang Chen*

Tianjin Key Laboratory of Applied Catalysis Science and Technology, Department of Catalysis Science and Engineering, School of Chemical Engineering and Technology, Tianjin University, Tianjin 300350, China



ARTICLE INFO

Keywords:
Ni-Ga alloy and intermetallic compound
Hydrodeoxygenation
Hydrogenation
C–C hydrogenolysis
Methanation

ABSTRACT

Herein, Ni/SiO₂ and bimetallic Ni_xGa/SiO₂ (Ni/Ga atomic ratio x = 6 and 3) catalysts were prepared by the impregnation method followed by reduction at 550 °C and tested in the vapor hydrodeoxygenation of anisole at 0.1 MPa and 300 °C. Ni-Ga alloy and Ni₃Ga intermetallic compound (IMC) formed in Ni₆Ga/SiO₂ and Ni₃Ga/SiO₂, respectively, where the Ga atoms break contiguous Ni ones reducing the ensembles of Ni atoms and the H₂ uptakes. Also, a charge transfer from Ga to Ni increased the electron density of Ni, and hydrogen spill-over occurred on Ni_xGa/SiO₂. In contrast to Ni/SiO₂, Ni_xGa/SiO₂ improved not only the hydrodeoxygenation activity but also the selectivity to benzene. At the similar anisole conversion (~31%), the selectivity to benzene was 75.2%, 83.0% and 92.6% on Ni/SiO₂, Ni₆Ga/SiO₂ and Ni₃Ga/SiO₂, respectively. Reactivity evaluation, anisole-TPD and TPSR results show that the direct C_{Ar}–OCH₃ bond cleavage (C_{Ar} represents the carbon in benzene ring) to benzene was more preferential on Ni_xGa/SiO₂ than on Ni/SiO₂. Isotope tracing experiment indicates that the spilt-over hydrogen at the interface between the Ni_xGa particles and support participated in the reaction. We suggest that the synergistic effect between Ni and Ga facilitated the direct C_{Ar}–O bond cleavage. Moreover, Ni_xGa/SiO₂ were less active for benzene hydrogenation and C–C bond hydrogenolysis than Ni/SiO₂, contributing to higher selectivity to benzene. Significantly, methanol, derived from the direct the C_{Ar}–OCH₃ bond cleavage, dominantly decomposed to CO and H₂ and methanation scarcely occurred on Ni_xGa/SiO₂, however, it was mainly converted to methane on Ni/SiO₂. Low activities for benzene hydrogenation, C–C bond hydrogenolysis and methanation on Ni_xGa/SiO₂ (especially Ni₃Ga/SiO₂) are attributed to the geometric and electronic effects of Ga in alloy and IMC. The finding is significant in rationally designing the catalyst with high benzene yield and low H₂ consumption.

1. Introduction

The accumulation of carbon dioxide in the atmosphere resulting from the extensive consumption of fossil fuels contributes to global warming. To alleviate this environmental issue, it has attracted great attention to develop renewable energy. Biomass is the only sustainable resource producing liquid fuels and chemicals [1]. Lignin, consisting of phenolic compounds with the weight up to 30% in lignocellulosic biomass, is a potential resource for aromatics (specifically, benzene, toluene and xylene (i.e., BTX)) [2]. Through fast pyrolysis and liquefaction, lignin is converted to bio-oil mainly containing phenolic compounds (such as phenol, anisole, guaiacol and cresol). Hydrodeoxygenation (HDO) is regarded as an effectively upgrading strategy to remove the oxygen in phenolics to produce aromatics. Generally, two

routes, i.e., direct deoxygenation (DDO) and hydrogenation-deoxygenation (HYD), take place during the HDO of phenolics [1,3,4]. In the DDO route, the C_{Ar}–O bond (C_{Ar} denotes carbon in benzene ring) of phenolics is directly cleaved to form aromatics. During the HYD pathway, a sequential hydrogenation-dehydration-hydrogenation reaction leads to hydrocarbons. Particularly, keto-enol tautomerization followed by hydrogenation-dehydration can also give rise to aromatics [1,5]. Additionally, transalkylation, C–C bond hydrogenolysis as well as methanation may simultaneously occur during HDO. Transalkylation is desirable due to increasing the carbon utilization, while C–C bond hydrogenolysis and methanation are undesirable because of the carbon loss and the increase of H₂ consumption. Contrast with the HYD route, the DDO one is more desirable because of higher aromatic yield and less H₂ consumption [6]. Reports have shown

* Corresponding author at: Department of Catalysis Science and Engineering, School of Chemical Engineering and Technology, Tianjin University, Tianjin 300350, China.

E-mail address: jxchen@tju.edu.cn (J. Chen).

that the catalyst property is a critical factor regulating the HDO route [2].

Supported CoMo and NiMo sulfides have been investigated for the HDO of phenolic compounds [7]. And CoMo sulfide is more beneficial to the DDO pathway than NiMo sulfide because it has more vacancies that are favorable for the vertical adsorption of phenolic through oxygen [7]. However, to keep sulfide catalysts from deactivation due to the sulfur loss, the sulfur-containing agents are required to add to the feedstock, consequently causing the sulfur contaminated products and the increase of the operation cost. As alternatives, noble metals (e.g., Ru, Pd, Pt, Re, and Rh) [8–11], base metals (e.g., Ni, Fe and Cu) [12,13], and metal phosphides [14,15] and carbides [16] have attracted attention. It has been found that noble metals and metallic Ni possess high HDO activity, however, some undesirable reactions, including the hydrogenation of benzene ring, C–C bond hydrogenolysis as well as methanation, also prevail on them, resulting in low aromatics yield and high H₂ consumption [17]. To circumvent these shortages, bimetallic catalysts have been focused, since the geometric/electronic properties of Ni or noble metals can be modified by another adjacent metal, and so the product selectivity is regulated. Interestingly, combining an oxophilic metal (e.g., Fe [18,19], Zn [10] and Re [9]) is very effective for the DDO pathway. Normally, the oxophilic metal atom is more preferential for adsorbing oxygen atom of phenolics, meanwhile, aromatic species is inclined to move away from the metal surface [9]. As a result, the C_{Ar}–O bond is readily activated while the benzene ring is unfavorably hydrogenated. For instance, adding Fe or Re to Ni/SiO₂ catalysts changes the main HDO product of cresol from 3-methyl cyclohexanone to toluene [5,9]. Furthermore, the C–C bond hydrogenolysis is remarkably suppressed on Ni-Re/SiO₂ [9]. Additionally, less oxophilic metals were also found to affect the catalyst reactivity. The introduction of metal In into Ni/SiO₂ increased the selectivity to BTX and inhibited the hydrogenation of benzene ring and C–C bond hydrogenolysis in the HDO of anisole [20]. The formation of Ni-Cu alloy enhanced the HDO rate of anisole, while the HYD pathway was still more dominating than the DDO one on Ni-Cu alloy [13].

Ga has been widely used to modify zeolites for improving dehydrogenation and aromatization [21]. Recently, Ga modified HZSM-5 and HBFA zeolites were found to be active for the HDO of benzaldehyde and m-cresol [6,22], and toluene and benzene were main products at high temperature (e.g., 500~550 °C). In the presence of H₂, highly dispersed GaH₂⁺/Ga⁺ species on Ga/HZSM-5 and Ga/HBFA contributed to the C–C and C–O bond hydrogenolysis. In the Ga-impregnated zeolites and SiO₂-supported Ga, the Ga-H species have also been found by the XANES technique [23]. Additionally, it has been reported that metal Ga can combine with Ni forming alloy and intermetallic compound (IMC) [24], where Ga modifies the geometric and electronic properties of Ni. To be specific, the Ga atoms break the contiguous Ni ones forming small Ni ensembles and makes the electron density of Ni increase due to a charge transfer from Ga to Ni. These remarkably enhanced the selectivity to alkenes in the selective hydrogenation of alkynes, ascribed to weakening the adsorption of electron-rich alkenes/alkynes on Ni-Ga alloy and IMC [24,25]. These results give us an inspiration, that is, Ni-Ga alloy and IMC are probably promising for the HDO of phenolics. Given that metal Ga was almost inert for hydrogenation [26], the isolation of electron-rich Ni atoms by the Ga ones is favorable for suppressing the C–C bond hydrogenolysis and benzene hydrogenation that are more preferential on larger ensemble of Ni atoms [20]. Also, the Ga species bearing positive charge are of electrophilic in nature and may interact with the oxygen atoms in the oxygenated compounds, and so they may not be a spectator and participate in the adsorption/activation of phenolics. All of these motivate us to explore the reactivity of Ni-Ga alloy and IMC in the HDO of phenolics.

In this work, we investigated the performance of SiO₂ supported Ni-Ga alloy and IMC catalysts for the HDO of anisole to produce benzene. In comparison with Ni/SiO₂, they promoted the cleavage of C_{Ar}–OCH₃

bond while suppressed the hydrogenation of benzene ring, C–C bond hydrogenolysis and methanation. To minimize the support effect, the relatively inert SiO₂ was used as support. Anisole was adopted as a model compound because it contains a typical phenolic structure (i.e., C_{CH3}–O–C_{Ar}).

2. Experimental

2.1. Catalyst preparation

Ni/SiO₂, Ga/SiO₂ and Ni_xGa/SiO₂ (x represents the Ni/Ga atomic ratio) catalysts were prepared by the incipient impregnation method. SiO₂ particles (0.15~0.25 mm) were incipiently impregnated by an aqueous solution containing Ni(NO₃)₂ and/or Ga(NO₃)₃, followed by drying at 120 °C for 12 h, calcination at 500 °C for 4 h in air and reduction with H₂ at 550 °C for 3 h. Before the reduced catalysts were exposed to air for some characterizations (such as XRD and XPS), they were passivated at room temperature with a 0.5% O₂/N₂ flow for 4 h. The nominal Ni mass contents in Ni/SiO₂ and Ni_xGa/SiO₂ were set as 10%. The nominal Ga mass content in Ga/SiO₂ was also set as 10%.

Additionally, a dual-layer catalyst system was denoted as Ni/Ga, where the Ni/SiO₂ particles were placed on the Ga/SiO₂ ones with the mass ratio of 1.

2.2. Catalyst characterization

H₂-TPR were used to characterize the reducibility of the calcined catalysts. The density of Ni sites and the state of adsorbed hydrogen on the reduced catalysts were measured by H₂ chemisorption and H₂-TPD, respectively. NH₃-TPD were adopted to investigate the catalyst acidity. The detail procedures for these characterizations are available in the Supplementary information.

X-ray diffraction (XRD) patterns were collected on a D8 X-ray diffractometer using Cu K α radiation ($\lambda = 0.1541$ nm). N₂ adsorption-desorption isotherms were got on a Quantachrom QuadraSorb SI instrument at –196 °C. The Brunauer-Emmett-Teller (BET) equation was used to calculate the specific surface area (S_{BET}). The pore volume (V_p) was estimated at a relative pressure of 0.99. The average pore diameter (d_p) was calculated using $d_p = 4V_p/S_{BET}$. X-ray photoelectron spectroscopy (XPS) was performed on a PHI 5000 VersaProbe instrument with Al K α radiation (1486.6 eV). Before the measurement, the passivated catalysts were sputter-cleaned with an Ar⁺ ion beam. Binding energies were calibrated by adventitious carbon (C1s at 284.8 eV)). The XPS spectra were resolved using the XPSPEAK41 software, during which a Shirley background was adopted, followed by peak fittings which were performed with Gaussia-Lorentzian profiles.

Thermogravimetric Analysis (TGA) of the fresh and used catalysts was conducted on a Mettler-Toledo TGA 1/SF instrument in an air flow (100 mL/min) at a temperature ramp rate of 10 °C/min.

Anisole-TPD was performed on a quartz tube reactor (inner diameter of 6 mm). 100 mg calcined catalyst was loaded into the reactor and reduced with a H₂ flow (60 mL/min) at 550 °C for 1 h, and then kept at 550 °C for 1 h to purge catalyst with a He flow (60 mL/min). And then it was cooled down to 50 °C and adsorbed anisole with the He flow containing anisole. After the adsorption of anisole, a purge with He was done to remove physically adsorbed anisole. Afterward, the catalyst was heated at a rate of 15 °C/min in the He flow (60 mL/min), and the effluent was monitored by a quadrupole mass spectrometer (HPR20, Hiden Analytic Ltd.).

Anisole-TPSR was also performed on a quartz tube reactor (inner diameter of 6 mm). 100 mg calcined catalyst was loaded into the reactor and reduced with a H₂ flow (60 mL/min) at 550 °C for 1 h. Afterward, two procedures were done. In the first case, the reduced catalyst was purged with a He flow (60 mL/min) at 550 °C for 1 h, and then cooled down to 50 °C and adsorbed anisole with the He flow containing anisole. In the second case, the reduced catalyst was directly

cooled down to 50 °C in the H₂ flow and then adsorbed anisole with the H₂ flow containing anisole. In both cases, after the adsorption of anisole, a purge with H₂ was done to remove physically adsorbed anisole. And then the catalyst was heated at a rate of 15 °C/min in the H₂ flow (60 mL/min), and the effluent was monitored by a quadrupole mass spectrometer (HPR20, Hiden Analytic Ltd.). In anisole-TPD and TPSR, the collected *m/z* signals included 108 (anisole), 94 (phenol), 84 (cyclohexane), 78 (benzene), 57 (n-petane and n-hexane), 43 (n-C₃~n-C₆ alkanes), 31 (methanol), 29 (formaldehyde or n-C₂~n-C₆ alkanes), 28 (CO or n-C₂~n-C₆ alkanes), 16 (CH₄) and 2 (H₂).

An isotope experiment was performed to investigate the role of spillover hydrogen on Ni₃Ga/SiO₂ for the HDO of anisole. 500 mg calcined Ni₃Ga/SiO₂ was loaded into a quartz-tube fixed-bed reactor (inner diameter of 6 mm) and reduced with a D₂ flow (60 mL/min) at 550 °C for 1 h, and then cooled to 300 °C and purged with a N₂ flow (60 mL/min) for 30 min to remove the D species on Ni₃Ga particles. After the mass signal of a quadrupole mass spectrometer was stable, an anisole/N₂ flow (60 mL/min) was passed through the catalyst bed for 30 min, and then the catalyst was heated at a rate of 15 °C/min in the anisole/N₂ flow, during which the *m/z* signals (17(CH₃D), 16(CH₄), 4(D₂), 3(HD) and 2(H₂)) were collected.

2.3. Reactivity test

The catalyst performance in the HDO of anisole was evaluated on an atmospheric quartz tube fixed-reactor (inner diameter of 6 mm). The calcined catalyst (0.15~0.25 mm in diameter) was placed on a quartz tool and 1.3 g quartz sand was placed on the catalyst bed. Before the test, the catalyst was reduced with a H₂ flow (100 mL/min) at 550 °C for 3 h, and then cooled to the reaction temperature. After the H₂ flow rate was adjusted to 48.9 mL/min, anisole was fed at a rate of 0.0098 mL/min using a micro pump and vaporized and mixed with H₂ before entering the reactor. The H₂/anisole molar ratio was 25. The weight hourly space velocity (WHSV) of anisole was regulated by changing the catalyst weight. The liquid effluent was trapped by octane in an ice water bath. Ethylbenzene was added into the liquid sample as an internal standard for quantitative analysis. The liquid samples were analyzed on a SP-3420 gas chromatography (GC) equipped with a flame ionization detector (FID) and a SE-30 capillary column (50 m × 0.32 mm × 3.0 μm). The C₁ gaseous products (i.e., CO, CO₂, and CH₄) were on-line analyzed on a 102 GC equipped with a TCD and a TDX-101 packed column, and N₂ was used as an internal standard. The C₁~C₅ gaseous hydrocarbons were on line analyzed on a SP-3420 GC equipped with a FID and a HP-AL/S capillary column (50 m × 0.535 mm × 15 μm). The representative chromatograms are shown in Fig. S1 in Supplementary Information.

The anisole conversion (*X*) and selectivity to product *i* containing 6~8 carbon atoms (*S_i*) and selectivity to product *j* containing 2~5 carbon atoms (*S_j*) were defined as follows:

$$X = (1 - n/n_0) \times 100\%$$

$$S_i = n_i/(n_0 - n) \times 100\%$$

$$S_j = kn_j/(n_0 - n) \times 100\%$$

where *n₀* and *n* denote the moles of anisole in the reactant and the effluent products, respectively; *n_i* and *n_j* denote the moles of product *i* and *j*, respectively. *k* represents the ratio between the carbon atom numbers in the product *j* and anisole.

Given that the conversions in this work were higher than 20%, far from differential conditions, the turnover frequency (TOF) of anisole was calculated by the integral equation [20]:

$$TOF = -F \times \ln(1-X)/(W \times 2M)$$

where *F* is the feed rate of anisole (μmol/s), *X* is the conversion of anisole, *W* is the weight of catalyst (g) and *M* is H₂ uptake (μmol/g).

This formula, in which -ln(1-X) substitutes for X, assumes a pseudo-first-order reaction, which is reasonable because the H₂ was large excessive. TOFs were calculated in absence of external/internal mass transfer limitations, justified by Mears and Weisz-Prater criterions (details in Supplementary Information).

3. Results and discussion

3.1. Catalyst characterization

3.1.1. Calcined catalysts

In the calcined Ni/SiO₂ and Ni_xGa/SiO₂, apart from amorphous SiO₂, only diffraction peaks due to NiO are observed at 37.3°, 43.3°, 62.9° and 75.4° (Fig. S2 in Supplementary Information), respectively corresponding to the (101), (012), (110) and (113) reflections of the face-centered cubic (fcc) NiO (PDF#71-1179). There was no Ga₂O₃ detected in the calcined Ga/SiO₂ and Ni_xGa/SiO₂, indicating that the Ga³⁺ species were highly dispersed and/or Ga₂O₃ was amorphous. It is also possible that the Ga³⁺ ions entered into the NiO lattice forming a solid solution because its radius (0.076 nm) is close to that (0.069 nm) of Ni²⁺ ion [27].

Fig. 1 shows the H₂-TPR profiles of the calcined catalysts. For the calcined Ni/SiO₂ that was completely reduced below 550 °C, the peak centered at ~380 °C with the shoulder at higher temperature are ascribed to the reductions of NiO and nickel silicate, respectively [28]. The calcined Ga/SiO₂ was initially reduced at ~290 °C, followed by a gradual reduction due to highly dispersed Ga₂O₃ and a broad peak centered at ~780 °C related to large Ga₂O₃ particles [22]. Clearly, Ga₂O₃ is more difficultly reduced than NiO, indicating that Ga is more oxophilic to oxygen than Ni. Compared with that of the calcined Ni/SiO₂, the peak assigned to NiO in the calcined Ni_xGa/SiO₂ shifted to higher temperature, that is, the reduction of NiO was suppressed due to the presence of Ga. Moreover, there are still peaks at the temperature higher than 550 °C for the calcined Ni_xGa/SiO₂, and the calcined Ni₃Ga/SiO₂ gave more peaks and higher terminal reduction temperature than the calcined Ni₆Ga/SiO₂. The peaks above 550 °C should be mainly attributed to the reduction of Ga species. Given the difficult reducibility of the calcined Ga/SiO₂, the presence of Ni facilitated the reduction of Ga³⁺ species in the calcined Ni_xGa/SiO₂ due to hydrogen spillover from reduced metallic Ni to Ga³⁺. The reduced Ga combined with metallic Ni forming the Ni-Ga alloy and IMC.

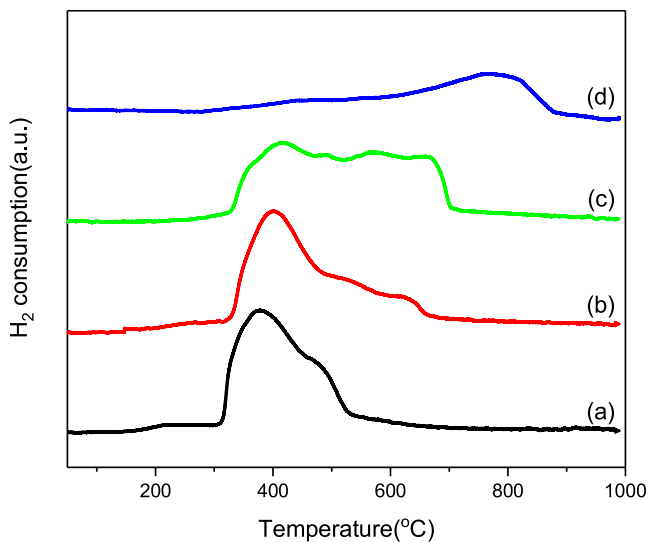


Fig. 1. H₂-TPR profiles of the calcined catalysts. (a) Ni/SiO₂; (b) Ni₆Ga/SiO₂; (c) Ni₃Ga/SiO₂; and (d) Ga/SiO₂.

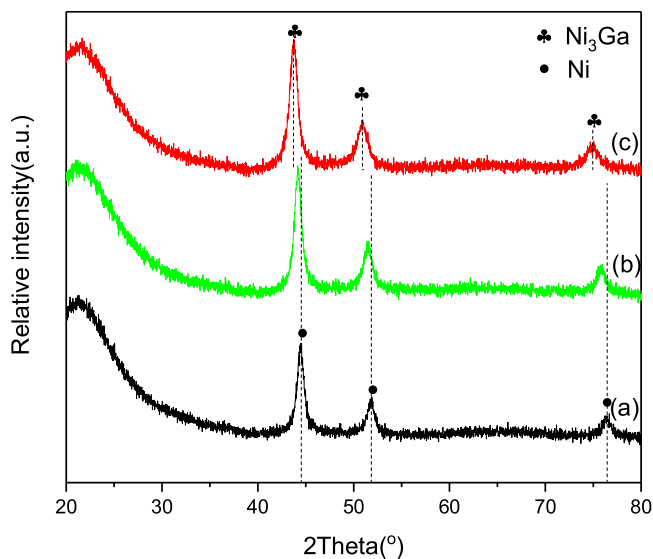


Fig. 2. XRD patterns of (a) Ni/SiO₂; (b) Ni₆Ga/SiO₂; (c) Ni₃Ga/SiO₂.

3.1.2. Reduced catalysts

Fig. 2 shows the XRD patterns of the Ni/SiO₂ and Ni_xGa/SiO₂ catalysts after reduction at 550 °C. The distinct diffraction peaks at 44.5°, 51.8° and 76.3° are observed for Ni/SiO₂, corresponding to the (111), (200), and (220) reflections of the metallic Ni with fcc structure (PDF#04-0850), respectively. Compared with those of Ni/SiO₂, the peaks due to metallic Ni slightly shifted to lower angles for Ni₆Ga/SiO₂. This indicates the incorporation of larger Ga atom (0.135 nm in radius) into the Ni lattice (Ni atom 0.125 nm in radius) [24], making the Ni unit cell expand, i.e., Ni-Ga alloy formed in Ni₆Ga/SiO₂. To further confirm this, Ni₆Ga/SiO₂ was re-calcined at 500 °C for 4 h. The resulting sample was performed for H₂-TPR, and it gave only one reduction peak centered at 448 °C (Fig. S3), very different from Ni₆Ga/SiO₂ before reduction (Fig. 1(b)). This indicates an intimate contact between Ni and Ga in the Ni-Ga alloy in Ni₆Ga/SiO₂. Particularly, the fcc Ni₃Ga IMC, with the peaks at 43.7°, 50.9° and 74.9° (PDF#65-3246), was detected in Ni₃Ga/SiO₂. In contrast to alloy where Ga atoms randomly distribute in Ni lattice, Ni₃Ga IMC, where the Ni atom is located at the face-centered position in the fcc structure, has more homogeneity of Ni and Ga [29,30]. Ni₃Ga/SiO₂ catalyst after re-calcination at 500 °C for 4 h also gave one dominating peak centered at 505 °C in its H₂-TPR profile (Fig. S3), very different from Ni₃Ga/SiO₂ before reduction (Fig. 1(c)). In short, the Ni-Ga alloy and Ni₃Ga IMC formed in Ni₆Ga/SiO₂ and Ni₃Ga/SiO₂, respectively, and there was a strong interaction between Ni and Ga. This is also verified by the charge transfer indicated by XPS in the following. Additionally, there were similar metallic Ni, Ni-Ga alloy and Ni₃Ga IMC crystallite sizes in the different catalysts (Table 1).

Table 1 shows the textural properties of the reduced catalysts. S_{BET}

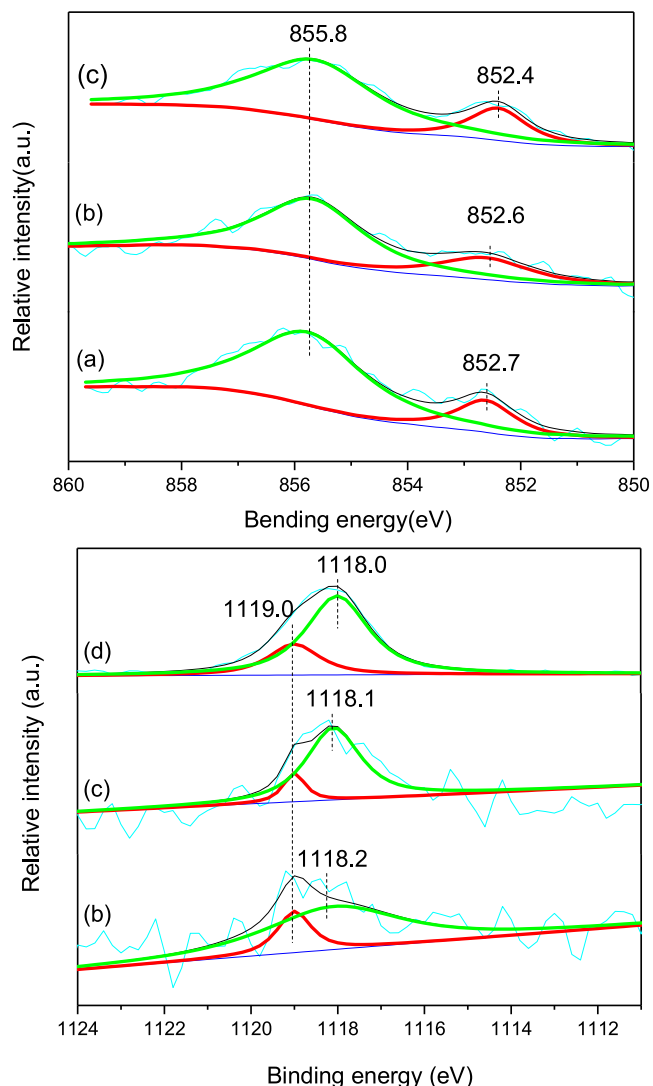


Fig. 3. XPS spectra in the ranges of (A) Ni 2p_{3/2} and (B) Ga 2p_{3/2}. (b) Ni/SiO₂; (b) Ni₆Ga/SiO₂; (c) Ni₃Ga/SiO₂; (d) Ga/SiO₂.

decreased from 462 to 408 m² g⁻¹ in the order of Ni/SiO₂, Ni₆Ga/SiO₂ and Ni₃Ga/SiO₂, while all the catalysts had similar pore volumes (0.61~0.69 cm³/g) and pore diameters (~5.7 nm).

The electronic interaction between Ni and Ga was investigated by XPS. As shown in Fig. 3(A), the Ni 2p_{3/2} binding energy (BE) of 855.8 eV and the Ga 2p_{3/2} BE of 1119.0 eV are assigned to Ni²⁺ species and Ga³⁺ species [31,32], respectively. Their presence is related to the catalyst passivation and/or the unreduced species. For Ni/SiO₂, Ni 2p_{3/2}

Table 1
Properties of Ni/SiO₂, Ga/SiO₂ and Ni_xGa/SiO₂ catalysts.

Catalyst	H ₂ uptake (μmol/g _{catal})	TOF (s ⁻¹)	Crystallite size (nm)		S _{BET} (m ² /g)	d _p (nm)	V _p (cm ³ /g)	Relative acid amount ^c		
			XRD ^a	XRD ^b				I ^d	II ^e	Total
Ni/SiO ₂	4.51	0.30	9.9	10.6	462	5.7	0.69	1.00	1.29	2.29
Ni ₆ Ga/SiO ₂	1.50	0.95	9.5	11.4	432	5.6	0.67	1.36	1.26	2.62
Ni ₃ Ga/SiO ₂	0.11	15.3	10.7	8.9	408	5.7	0.61	1.50	1.48	2.98
Ga/SiO ₂	0.00	–	–	–	425	5.7	0.65	–	–	8.10

^a Crystallite size in calcined samples calculated using the Scherrer equation based on the NiO (111) reflection.

^b Crystallite size calculated using the Scherrer equation based on the Ni(111) or Ni₃Ga(111) reflection.

^c The weak acid amount of Ni/SiO₂ was designed as 1.00.

^d First peak (attributed to weak acidity) centered at ~270 °C.

^e Second peak (attributed to medium acidity) centered at 320 °C for Ni/SiO₂, 340 °C for Ni₆Ga/SiO₂ and 360 °C for Ni₃Ga/SiO₂.

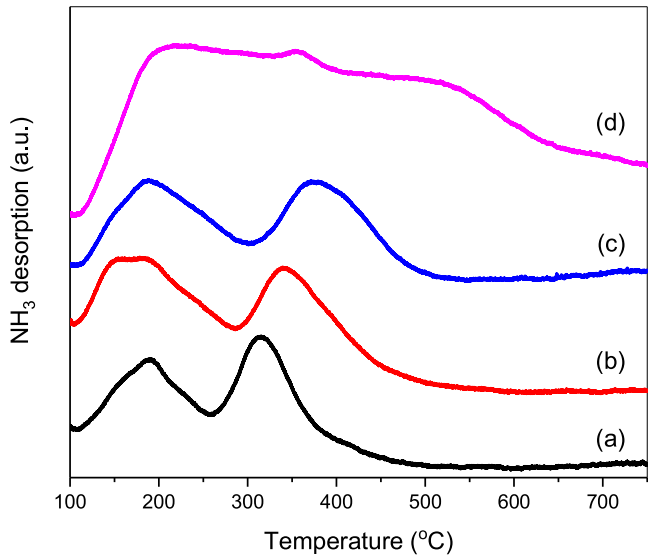


Fig. 4. NH₃-TPD profiles of (a) Ni/SiO₂; (b) Ni₆Ga/SiO₂; (c) Ni₃Ga/SiO₂; (d) Ga/SiO₂.

2 BE of 852.7 eV is attributed to metallic Ni [33,34]. By contrast, Ni₆Ga/SiO₂ and Ni₃Ga/SiO₂ had lower Ni 2p_{3/2} BEs (852.6 and 852.4 eV, respectively), indicating a charge transfer from Ga to Ni, consistent with the result from EXAFS [26]. This is reasonable because Ni has larger electronegativity (1.9) than Ga (1.8). Indeed, as shown in Fig. 3(B), the Ga 2p_{3/2} BEs (~1118.2 eV) in Ni_xGa/SiO₂ were lower than ~1119.0 eV attributed to Ga³⁺ but higher than 1117.0 eV attributed to metallic Ga [35], i.e., the Ga species in Ni_xGa/SiO₂ possessed a positive charge. Particularly, apart from that of 1119.0 eV, the Ga 2p_{3/2} BE of 1118.0 eV was found in Ga/SiO₂, which is assigned to Ga⁺ species [32]. That is, Ga₂O₃ was reduced to Ga₂O (Eq. (1)) [6]. Indeed, as shown in H₂-TPR profile (Fig. 1), a part of Ga₂O₃ could be reduced at 550 °C. This case has also been reported for the Ga-modified H-Beta and HZSM-5 zeolites treated with H₂ at 400–550 °C [22].



The NH₃-TPD profiles of the catalysts are shown in Fig. 4. For Ga/SiO₂, there was a large broad peak between 110 and 600 °C, indicative of a large acid amount. On one hand, the reduced and unreduced Ga species (i.e., Ga⁺ and Ga³⁺) acted as Lewis sites. On the other hand, the Ga³⁺ ions might bond tetrahedrally on the SiO₂ surface, and the generated bridging hydroxyl groups between Ga³⁺ and Si⁴⁺ could serve as Brønsted acid sites [36,37]. Two peaks at about 170 and 320 °C, respectively corresponding to weak and medium acid sites, appeared in the profile of Ni/SiO₂, which is related to the unreduced Ni species [38]. In the profiles of Ni_xGa/SiO₂ catalysts, the peak at about 170 °C is still visible, while the second peak shifted to higher temperature (340 °C for Ni₆Ga/SiO₂; 360 °C for Ni₃Ga/SiO₂) in comparison with Ni/SiO₂. Also, the amounts of both weak and medium acid sites increased in the order of Ni/SiO₂, Ni₆Ga/SiO₂, Ni₃Ga/SiO₂, and Ga/SiO₂ (Table 1). Thus, the presence of Ga increased the catalyst acidity. This should be mainly attributed to the charge transfer from Ga to Ni, producing positively charged Ga species as Lewis acid sites [24,36].

H₂ chemisorption was adopted to measure the surface density of Ni atoms. Ni/SiO₂ gave the H₂ uptake of 4.51 μmol/g. By contrast, Ni₆Ga/SiO₂ and Ni₃Ga/SiO₂ had very lower uptakes (1.5 and 0.11 μmol/g, respectively). This is reasonable because of the formation of Ni-Ga alloy and Ni₃Ga IMC. In Ni-Ga alloy and Ni₃Ga IMC, the ensembles of the Ni atoms were reduced due to the isolation of Ga, according with the structure property of alloy and IMC [29]. This consequently reduces the density of the surface Ni atoms because there were the similar Ni-Ga alloy and Ni₃Ga IMC crystallite sizes in Ni_xGa/SiO₂ to the metallic Ni

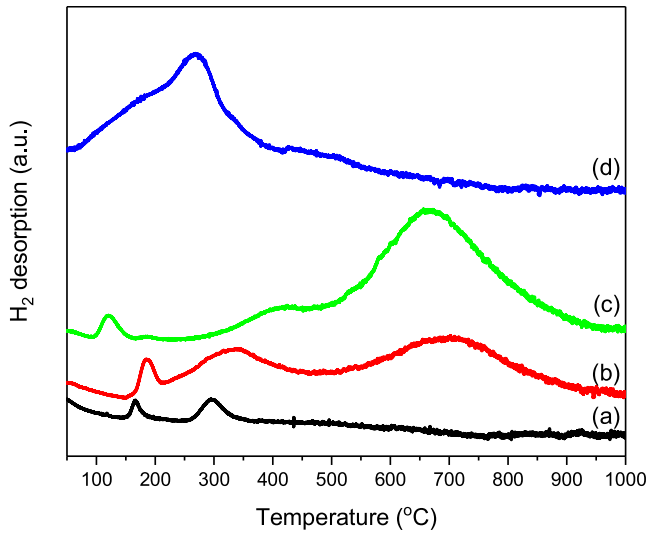
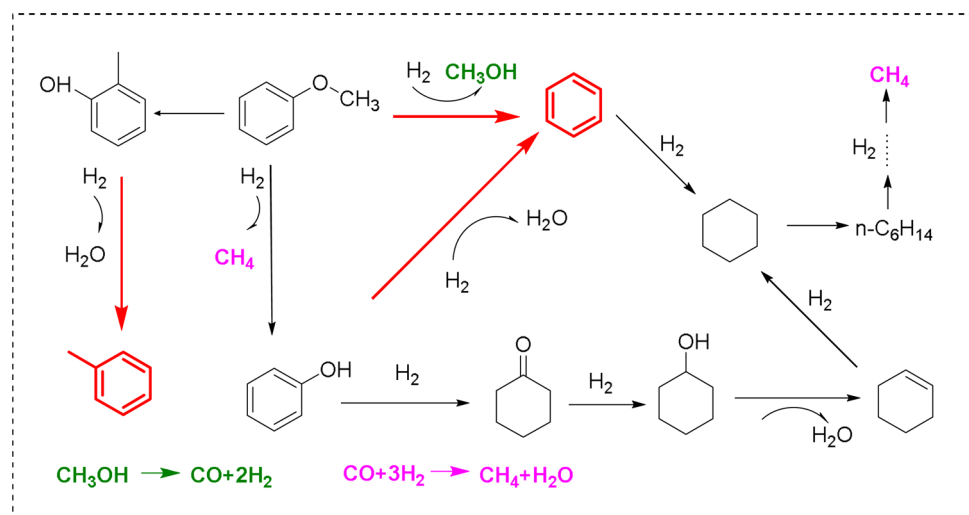


Fig. 5. H₂-TPD profiles of (a) Ni/SiO₂; (b) Ni₆Ga/SiO₂; (c) Ni₃Ga/SiO₂; (d) Ga/SiO₂.

one in Ni/SiO₂ (Table 1). Additionally, H₂ uptake on Ga/SiO₂ was zero.

H₂-TPD was also carried out to investigate the state of hydrogen adsorbed on the catalysts (Fig. 5). For Ni/SiO₂, two small peaks (centered at 170 and 300 °C) below 400 °C are ascribed to the desorption of hydrogen on metallic Ni [28,39]. A large broad peak below 400 °C is visible for Ga/SiO₂. This is attributed to the partial reduction of Ga/SiO₂ to produce Ga⁺ species as indicated by XPS. It has been reported that the Ga-H species formed on the Ga/SiO₂ surface after H₂ treatment above 500 °C, during which heterolytic cleavage of H₂ on Ga-O bond gave rise to a Ga-H bond by replacing a Ga-O bond [23,40]. Meanwhile, the hydrides (i.e., GaH₂³⁺ and GaH₂⁺) might also form [22]. The Ga-H species and hydrides contribute to the H₂ desorption peak for Ga/SiO₂. Ni₆Ga/SiO₂ gave two peaks at ~186 and 333 °C below 400 °C. Apart from a peak at ~120 °C on Ni₃Ga/SiO₂, there was also a peak that started at ~270 °C and centered at ~416 °C. Given that Ga-H species might form, the desorbed H₂ below 400 °C on Ni_xGa/SiO₂ may be not only from the Ni atoms. Interestingly, Ni_xGa/SiO₂ gave very large peaks above 400 °C (centered at ~703 and 667 °C for Ni₆Ga/SiO₂ and Ni₃Ga/SiO₂, respectively), which is generally attributed to spilt-over hydrogen species on support that are distant from metal particles [41]. By contrast, the spilt-over hydrogen species at the metal-support interface more easily desorb (usually at 300–400 °C) [42,43]. Here, as to Ni_xGa/SiO₂, given that the Ga-H species may exist, we tentatively assign the peaks at 330 °C for Ni₆Ga/SiO₂ and 416 °C for Ni₃Ga/SiO₂ to the adsorbed H₂ at the metal-support interface and on Ga atom. As found by Connell et al [37], Ga³⁺ can bond tetrahedrally on the SiO₂ surface generating bridging hydroxyl groups, while hydroxyl groups may act as a reservoir of spilt-hydrogen species [44]. This may account for more spilt-over hydrogen species on Ni_xGa/SiO₂.

As indicated above, the H₂ chemisorption and H₂-TPD gave very different information about H₂ adsorption. Measured by the H₂ chemisorption, Ni/SiO₂ gave very larger H₂ uptake than Ni_xGa/SiO₂. However, as indicated by H₂-TPD, the difference between the amounts of H₂ desorbed from Ni_xGa/SiO₂ and Ni/SiO₂ below 350 °C was not so large as that of their H₂ uptakes. The H₂ uptake was determined by a pulse technique, during which the reduced catalyst was purged with N₂ at the reduction temperature (i.e., 550 °C) to remove the adsorb H species on metal sites and the pulsed H₂ quickly passed through the catalyst bed at 30 °C. Differently, before H₂-TPD, no N₂ purge at 550 °C was done for the reduced catalyst and the reduced catalyst was cooled down to 30 °C in H₂ and then further adsorbed H₂ for 30 min at 30 °C. That is, there was an enough time for H₂ adsorption on metal sites (including on the Ga sites forming the Ga-H species) before H₂-TPD.



Scheme 1. Proposed reaction pathway in HDO of anisole (Red arrows denote the DDO pathway).

Thus, the formation of Ni-Ga alloy and IMC (especially the latter) reduced the ability of Ni for quick H₂ adsorption/activation. This is also evidence by anisole-TPSR on Ni₃Ga/SiO₂ with or without purging with He at 550 °C (in Section 3.3).

3.2. Catalytic reactivity

The performance of Ni/SiO₂ and Ni_xGa/SiO₂ catalysts in the HDO of anisole were tested at 300 °C, 0.1 MPa and different WHSVs (1.0~4.0 h⁻¹). The main products were benzene, phenol, cyclohexane, CO and CH₄. The others include cyclohexanone, cyclohexanol, hexene, n-C₂~n-C₆ alkanes, cresol, toluene and methanol. As indicated in the literatures [1,8], there were two routes in the HDO of anisole (i.e., DDO and HYD). Here, given the product distribution, we proposed a reaction pathway in the HDO of anisole (shown in Scheme 1). The DDO pathway involves the direct cleavage of the C_{Ar}—O bond. The cleavage of C_{Ar}—OCH₃ bond produces benzene and methanol. Methanol can decompose to CO and H₂. Additionally, the cleavage of O—C_{CH3} bond produces phenol, which can be converted either to benzene via the DDO pathway or to cyclohexanone and cyclohexanol via the hydrogenation of benzene ring (i.e., HDY pathway). Cyclohexanol is further converted to cyclohexane via dehydration-hydrogenation. Cyclohexane can also be generated from the hydrogenation of benzene, during which hexene may be an intermediate. The ring open of cyclohexane followed by the further C—C bond hydrogenolysis gives rise to C₁~C₆ alkanes. CH₄ can also be produced from CO methanation. In addition, cresol is derived from the methyl transfer of anisole, and then it is converted to toluene via the DDO pathway.

The anisole conversions on Ni/SiO₂ and Ni_xGa/SiO₂ were shown in Fig. 6(A). With increasing WHSV from 1.0 to 4.0 h⁻¹, the anisole conversions decreased on all the catalysts (from 69.9% to 23.2% on Ni/SiO₂, from 59.2% to 24.1% on Ni₆Ga/SiO₂ and from 71.8% to 27.6% on Ni₃Ga/SiO₂) due to the shortened contact time. At the same WHSV, the anisole conversion tended to increase in the order of Ni/SiO₂, Ni₆Ga/SiO₂ and Ni₃Ga/SiO₂ (apart from higher on Ni/SiO₂ than on Ni₆Ga/SiO₂ at the WHSV of 1.0 h⁻¹). That is, Ni_xGa/SiO₂ (especially Ni₃Ga/SiO₂) were more active than Ni/SiO₂. Based on the H₂ uptakes, anisole TOFs were estimated to indicate the activity of per surface Ni site. As shown in Table 1, Ni_xGa/SiO₂ had larger TOFs than Ni/SiO₂, and Ni₃Ga/SiO₂ gave the largest one (15.3 s⁻¹). It has been reported in literatures that TOFs of anisole are between 0.0061 and 4.58 s⁻¹ on different catalysts (Table S1). Compared with that of Ni/SiO₂, the higher activity of Ni_xGa/SiO₂ is ascribed to a synergistic effect between Ni and Ga discussed in Section 3.3.1.

The selectivities to main liquid products are also displayed in

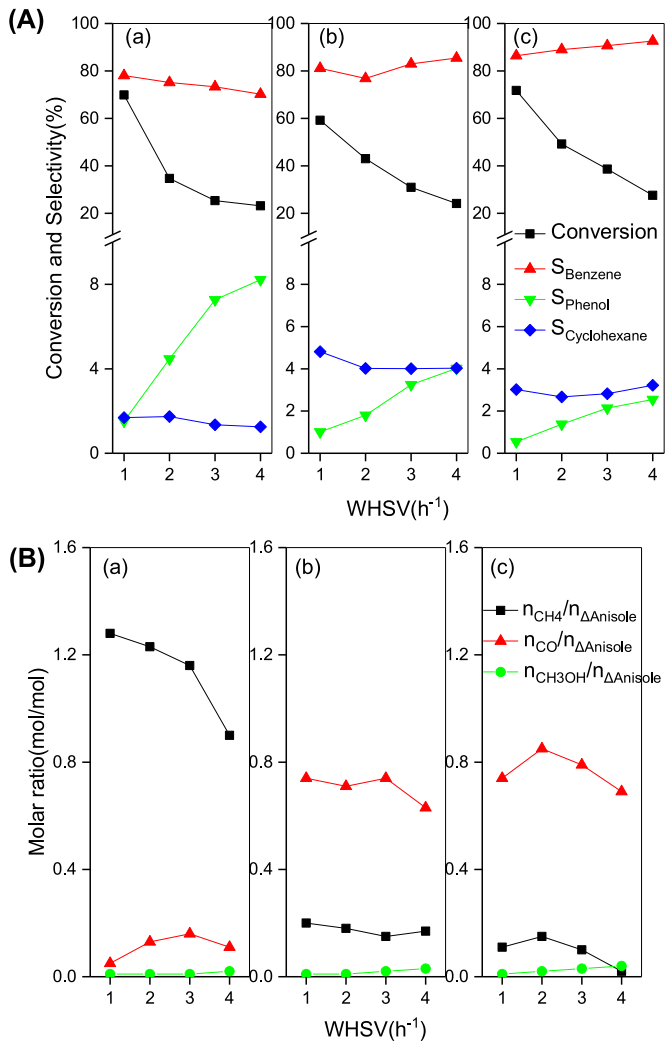


Fig. 6. (A) Anisole conversion and product selectivity; and (B) n_{CH3OH}/n_{ΔAnisole}, n_{CO}/n_{ΔAnisole} and n_{CH4}/n_{ΔAnisole} molar ratios as a function of WHSV. (a) Ni/SiO₂, (b) Ni₆Ga/SiO₂ and (c) Ni₃Ga/SiO₂. Reaction condition: 300 °C, 0.1 MPa, H₂/anisole molar ratio of 25.

Fig. 6(A). Benzene was the main HDO product on all the catalysts, and Ni_xGa/SiO₂ gave higher selectivity to benzene (S_{benzene}) than Ni/SiO₂ at the same WHSV. Interestingly, as WHSV increased from 1.0 to 4.0 h⁻¹,

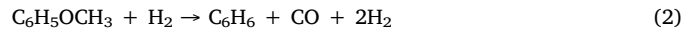
the selectivity to benzene decreased from 78.1% to 70.2% on Ni/SiO₂, while it increased from 81.1% to 85.4% on Ni₆Ga/SiO₂ and from 86.4% to 92.6% on Ni₃Ga/SiO₂. Phenol was detected as the main intermediate. With increasing WHSV from 1.0 to 4.0 h⁻¹, the selectivity to phenol increased on all the catalysts (from 1.52% to 8.22% on Ni/SiO₂, from 1.01% to 4.02% on Ni₆Ga/SiO₂ and from 0.54% to 2.55% on Ni₃Ga/SiO₂). At the same WHSV, the selectivity to phenol decreased in the order of Ni/SiO₂, Ni₆Ga/SiO₂ and Ni₃Ga/SiO₂. Relatively, benzene and phenol were more preferentially produced on Ni_xGa/SiO₂ (especially Ni₃Ga/SiO₂) and Ni/SiO₂, respectively.

As shown in **Scheme 1**, the cleavage of C_{Ar}—OCH₃ bond leads to benzene and methanol, while the cleavage of O—CH₃ bond gives rise to phenol and CH₄. Furthermore, methanol can decompose to CO and H₂, and CO can further be hydrogenated to CH₄. Here, the amounts of formed methanol, CO and CH₄ are represented by the molar ratios of methanol, CO and CH₄ to the converted anisole (denoted as n_{CH3OH}/n_{Δanisole}, n_{CO}/n_{Δanisole} and n_{CH4}/n_{Δanisole}, respectively), respectively. As shown in **Fig. 6(B)**, the n_{CH3OH}/n_{Δanisole} molar ratio was very low (0.01~0.04) on all the catalysts, ascribed to the easy decomposition of methanol as indicated in the following text. By contrast, the n_{CO}/n_{Δanisole} and n_{CH4}/n_{Δanisole} molar ratios were higher. At WHSV of 1.0~4.0 h⁻¹, Ni/SiO₂ gave the n_{CH4}/n_{Δanisole} molar ratio of 1.28~0.9 and the n_{CO}/n_{Δanisole} molar ratio of 0.05~0.11. In contrast, the n_{CH4}/n_{Δanisole} ratio ranged from 0.15 to 0.20 on Ni₆Ga/SiO₂ and from 0.02 to 0.15 on Ni₃Ga/SiO₂, much lower than that on Ni/SiO₂. Interestingly, the n_{CO}/n_{Δanisole} ratio ranged from 0.63 to 0.74 on Ni₆Ga/SiO₂ and from 0.69 to 0.85 on Ni₃Ga/SiO₂, much higher than that on Ni/SiO₂. Clearly, in the order of Ni/SiO₂, Ni₆Ga/SiO₂ and Ni₃Ga/SiO₂, the n_{CO}/n_{Δanisole} ratio increased while the n_{CH4}/n_{Δanisole} ratio decreased. Given that CO is only generated from the decomposition of CH₃OH and the n_{CH3OH}/n_{Δanisole} molar ratio was very low, a higher n_{CO}/n_{Δanisole} ratio indicates that the C_{Ar}—OCH₃ bond was more preferentially cleaved. Therefore, it is certain that benzene was mainly produced via the cleavage of C_{Ar}—OCH₃ bond on Ni_xGa/SiO₂. As to Ni/SiO₂, benzene could also be yielded through the cleavage of C_{Ar}—OCH₃ bond because of the formation of methanol and CO. Herein, there was an obvious separation of water from oil phase in the liquid effluent on Ni/SiO₂, however, water was almost invisible in the liquid effluent on Ni_xGa/SiO₂, indicative of very small of water formed on Ni_xGa/SiO₂. One of routes forming water is CO methanation on Ni/SiO₂. This also means that the removed oxygen existed mainly in forms of water and CO on Ni/SiO₂ and Ni_xGa/SiO₂, respectively. Given that the decomposition of methanol followed by the CO methanation may take place, Ni/SiO₂ and Ni₃Ga/SiO₂ were evaluated for the methanol conversion in the H₂ atmosphere on a fixed-bed reactor at 300 °C, 0.1 MPa, H₂/methanol molar ratio of 25 and methanol WHSV of 4 h⁻¹. It was found that Ni₃Ga/SiO₂ gave lower methanol conversion (63.3%) than Ni/SiO₂ (98.4%). Only CO was detected in the gaseous effluent on Ni₃Ga/SiO₂, that is, methanol decomposed to CO while no methanation took place. However, both CO and CH₄ (with the molar ratio of 1.6) formed on Ni/SiO₂, i.e., CO methanation took place. This is reasonable because metallic Ni is very active for methanation [17]. Clearly, methanol decomposition and CO methanation more easily occurred on Ni/SiO₂ than on Ni₃Ga/SiO₂. Therefore, it cannot be excluded that benzene was also mainly yielded via the cleavage of C_{Ar}—OCH₃ bond on Ni/SiO₂, which is confirmed by the anisole-TPSR (in Section 3.3). Even though, we deem that the cleavage of C_{Ar}—O bond is more preferential on Ni_xGa/SiO₂ (especially Ni₃Ga/SiO₂) in comparison with Ni/SiO₂. The evidences include: 1) with increasing WHSV, the selectivity to benzene increased on Ni_xGa/SiO₂ while decreased on Ni/SiO₂; 2) there was a lower selectivity to phenol on Ni_xGa/SiO₂.

It is worth noting that the n_{CH4}/n_{Δanisole} ratio exceeded 1.0 on Ni/SiO₂ at WHSV of 1~3 h⁻¹. This indicates that CH₄ was not only derived from the —OCH₃ group of anisole. Part of CH₄ should be produced from the benzene ring, during which a consecutive reaction, i.e., benzene→cyclohexane→hexane→...→CH₄, took place (**Scheme 1**). To verified

this, the hydrogenation of benzene on Ni/SiO₂ was tested on a fixed-bed reactor at 300 °C and 0.1 MPa (detail in Supplementary information). For comparison, Ni₃Ga/SiO₂ was also evaluated. As shown in **Fig. S4**, Ni₃Ga/SiO₂ gave very lower benzene conversion (9.3%) than Ni/SiO₂ (17.0%). Only the C₆ alkanes (i.e., cyclohexane and hexane with the selectivity of 97.1% and 2.6%, respectively) formed on Ni₃Ga/SiO₂. However, CH₄ with the selectivity of 68.8% was dominating on Ni/SiO₂, followed by C₂~C₅ alkanes (16.1%), cyclohexane (13.3%) and hexane (1.84%). Obviously, Ni₃Ga/SiO₂ possessed very lower activity for both the hydrogenation of benzene and the C—C bond hydrogenolysis than Ni/SiO₂. This also contributes to higher selectivity to benzene on Ni₃Ga/SiO₂ in the HDO of anisole, and can account for higher selectivity to cyclohexane on Ni_xGa/SiO₂ than on Ni/SiO₂ (**Fig. 6(A)**). In addition, because hexane was difficultly generated via the ring open of cyclohexane on Ni_xGa/SiO₂ while it was easily further converted via C—C bond hydrogenolysis on Ni/SiO₂, the selectivity to hexane was very low (0~0.14%) on Ni/SiO₂ and Ni_xGa/SiO₂. The selectivity to C₂~C₅ alkanes was also very low (< 1%) on all the catalysts in the HDO of anisole, attributed to that the C—C hydrogenolysis was difficult on Ni_xGa/SiO₂ while it was easy to produce CH₄ on Ni/SiO₂.

It is worth highlighting that benzene and CO were main products on Ni_xGa/SiO₂, while benzene and methane were dominating on Ni/SiO₂. As indicated in Eqs. (2) and (3), when 1 mol benzene and 1 mol CO were produced, 1 mol H₂ was simultaneously generated; however, 2 mol H₂ was consumed when 1 mol benzene and 1 mol CH₄ were produced. Clearly, also given lower activities for benzene hydrogenation and C—C bond hydrogenolysis on Ni_xGa/SiO₂ than those on Ni/SiO₂, H₂ consumption was significantly reduced on Ni_xGa/SiO₂ (especially Ni₃Ga/SiO₂) in the HDO of anisole.



There was a small amount of cyclohexanone formed on all the catalysts. Ni/SiO₂ possessed higher selectivity to cyclohexanone (0.2~1.0%) than Ni₆Ga/SiO₂ and Ni₃Ga/SiO₂ (< 0.2%) (**Fig. S5**), indicating that Ni/SiO₂ was more active for the hydrogenation of benzene ring in phenol. Trace cyclohexanol and hexene (< 1%) were detected on all the catalyst. Additionally, there were very low selectivities to cresol and toluene (0.4~1.3%) on all the catalysts (**Fig. S5**), that is, the catalyst acidity is not enough to catalyze the methyl transfer of anisole.

Fig. 7 shows the selectivities to the main products, n_{CO}/n_{Δanisole} and n_{CH4}/n_{Δanisole} molar ratios on Ni/SiO₂ and Ni_xGa/SiO₂ at the similar anisole conversions (31 ± 4%). Same to the above, compared with Ni/SiO₂, Ni_xGa/SiO₂ gave higher selectivities to benzene and cyclohexane and lower selectivities to phenol and cyclohexanone. The main gaseous product was CH₄ on Ni/SiO₂ while CO on Ni_xGa/SiO₂. In short, Ni_xGa/SiO₂ (especially Ni₃Ga/SiO₂) possessed better performance than Ni/SiO₂, giving rise to higher benzene yield and lower H₂ consumption. This is mainly due to the formation of Ni-Ga alloy and Ni₃Ga IMC.

3.3. Anisole-TPD and TPSR

Given the product distribution on Ni/SiO₂ and Ni_xGa/SiO₂ in the HDO of anisole (**Fig. 6**), the direct cleavage of the C_{Ar}—OCH₃ bond was more favorable on Ni_xGa/SiO₂ than on Ni/SiO₂. To provide more information about the reaction mechanism, anisole-TPD and anisole-TPSR on Ni/SiO₂ and Ni₃Ga/SiO₂ were carried out.

Fig. 8 shows anisole-TPD profiles on Ni/SiO₂ and Ni₃Ga/SiO₂. A broad anisole desorption peak between 150 and 600 °C is visible for both catalysts. Meanwhile, H₂, CO and CH₄ were monitored. For Ni/SiO₂, H₂ was initially produced at ~313 °C with a distinct peak centered at 347 °C and a broad peak spanned from 430 to 780 °C, CO was primarily produced in a peak centered at 313 °C and a shoulder at ~347 °C, while CH₄ was produced in a peak centered at ~347 °C. As to Ni₃Ga/SiO₂, H₂ primarily desorbed above 400 °C, CO desorbed in a distinct

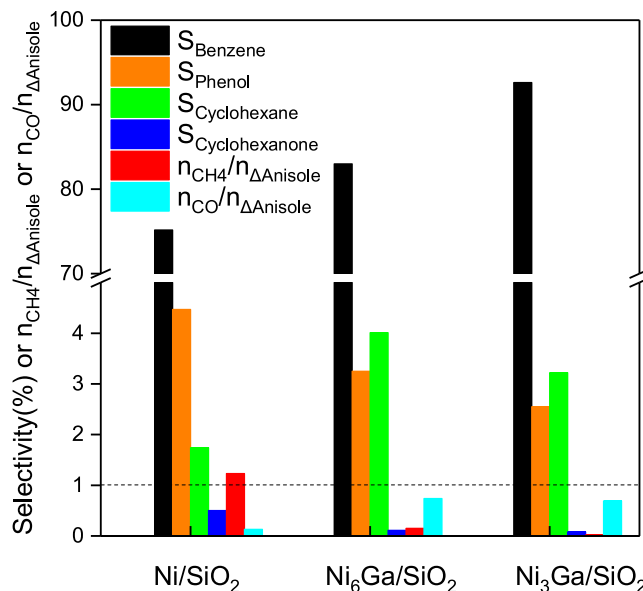


Fig. 7. Product distribution on Ni/SiO₂, Ni₆Ga/SiO₂ and Ni₃Ga/SiO₂ at similar anisole conversion ($31 \pm 4\%$). Reaction condition: 300 °C, 0.1 MPa, H₂/anisole molar ratio of 25.

peak at 432 °C and a shoulder at 450 °C, and CH₄ was produced in a peak centered at 450 °C. Clearly, the onset of the primary H₂, CO and CH₄ desorption features occurred at higher temperatures (> 100 °C) on Ni₃Ga/SiO₂ than on Ni/SiO₂. It has been reported that H₂, CO and CH₄ were produced from the scission of the C—H, C_{Ar}—O and O—CH₃ bonds in adsorbed anisole [10], respectively. Thus, the presence of Ga reduced the activity for the scission of C—H and C—O bonds. Interestingly, the desorption peak of CH₄ was larger than that of CO on Ni/SiO₂, while it was much smaller than that of CO on Ni₃Ga/SiO₂. This indicates that the O—CH₃ and C_{Ar}—OCH₃ bond in the adsorbed anisole were preferentially broken on Ni/SiO₂ and Ni₃Ga/SiO₂, respectively.

The anisole-TPSR on Ni/SiO₂ and Ni₃Ga/SiO₂ were carried out in two cases, i.e., the reduced catalysts were purged with He at the reduction temperature (i.e., 550 °C) (Fig. 9) and not purged with He (Fig. 10). As shown in Fig. 9, for Ni/SiO₂, benzene and methanol, derived from the scission of the C_{Ar}—OCH₃ group, were simultaneously

generated and reached maximum at the similar temperature (~156 °C). Meanwhile, the CH₂O and CO peaks at ~156 °C likely resulted from the dehydrogenation of methanol and the decomposed of CH₂O, respectively. At the similar temperature, methane was also produced, likely from the scission of the O—CH₃ group and CO methanation. No phenol was simultaneously monitored with methane, probably due to the small amount of formed phenol and the strong adsorption of phenol on the catalyst surface. Phenol has been reported to be more strongly adsorbed on the catalyst surface than anisole [45,46]. Apart from cyclohexane, other alkane fragment ions (*m/z* = 57 for petane and hexane; *m/z* = 43 for n-C₃~n-C₆ alkanes; *m/z* = 29 for n-C₂~n-C₆ alkanes; *m/z* = 28 for n-C₂~n-C₆ alkanes) were also monitored, all of which appear after the peak (156 °C) due to benzene. Cyclohexane and C₂~C₆ alkanes were simultaneously monitored with the peaks at ~193 and ~280 °C, and CH₄ was always monitored above 156 °C, indicating that the consecutive reaction (benzene→cyclohexane→hexane→...→CH₄) quickly took place. This indicates that benzene was immediately hydrogenated after produced. Given simultaneous desorption of the C₂~C₆ alkanes, the peaks at ~193 and ~280 °C are scarcely related to CH₂O and CO. At above ~350 °C, apart from benzene with the gradually decreased signal, there was almost only CH₄ monitored, indicating that the formed benzene was immediately hydrogenated followed by hydrogenolysis and completely converted to CH₄ at such high temperature. By contrast, for Ni₃Ga/SiO₂, there were no benzene, cyclohexane, n-C₂~n-C₆ alkanes, methanol, CH₂O, CO, and CH₄ monitored below ~170 °C, which is related to lower H₂ adsorption/activation ability of Ni₃Ga IMC than metallic Ni at low temperature as indicated in the H₂-TPD section. Interestingly, benzene was initially monitored at ~170 °C with a large broad peak centered at ~350 °C, accompanying with the formation of methanol, CH₂O and CO, ascribed to the cleavage of C_{Ar}—OCH₃. Small peaks due to cyclohexane (at 300 °C) and C₃~C₆ alkanes (at 248 °C) mean that the benzene hydrogenation and the C—C bond hydrogenolysis were difficult on Ni₃Ga/SiO₂. Thus, the cleavage of C_{Ar}—OCH₃ bond to form benzene may be reaction limited. Furthermore, CH₄ was mainly monitored at above 380 °C, much lower than that (> 120 °C) on Ni/SiO₂. Thus, the O—CH₃ bond cleavage and the C—C bond hydrogenolysis are more favorable on Ni/SiO₂ than on Ni₃Ga/SiO₂.

As shown in Fig. 10, for Ni/SiO₂ without He purge, the desorption features of the products are similar with those purged with He. For Ni₃Ga/SiO₂, different from the case purged with He, a small peak due to benzene is observed at 140 °C, accompanying with the formation of

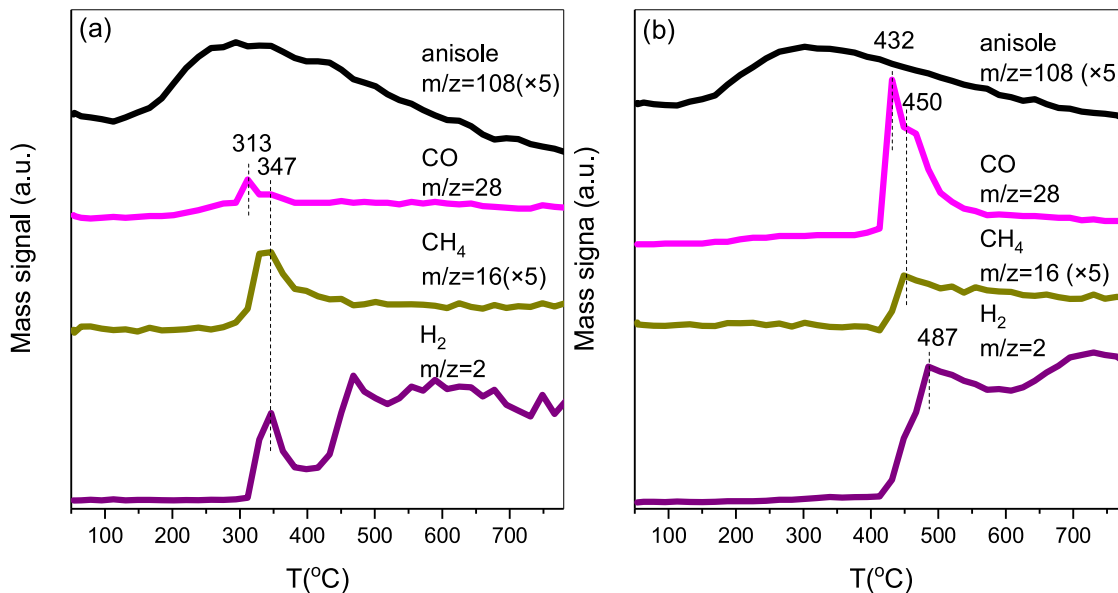


Fig. 8. Anisole-TPD on (a) Ni/SiO₂ and (b) Ni₃Ga/SiO₂.

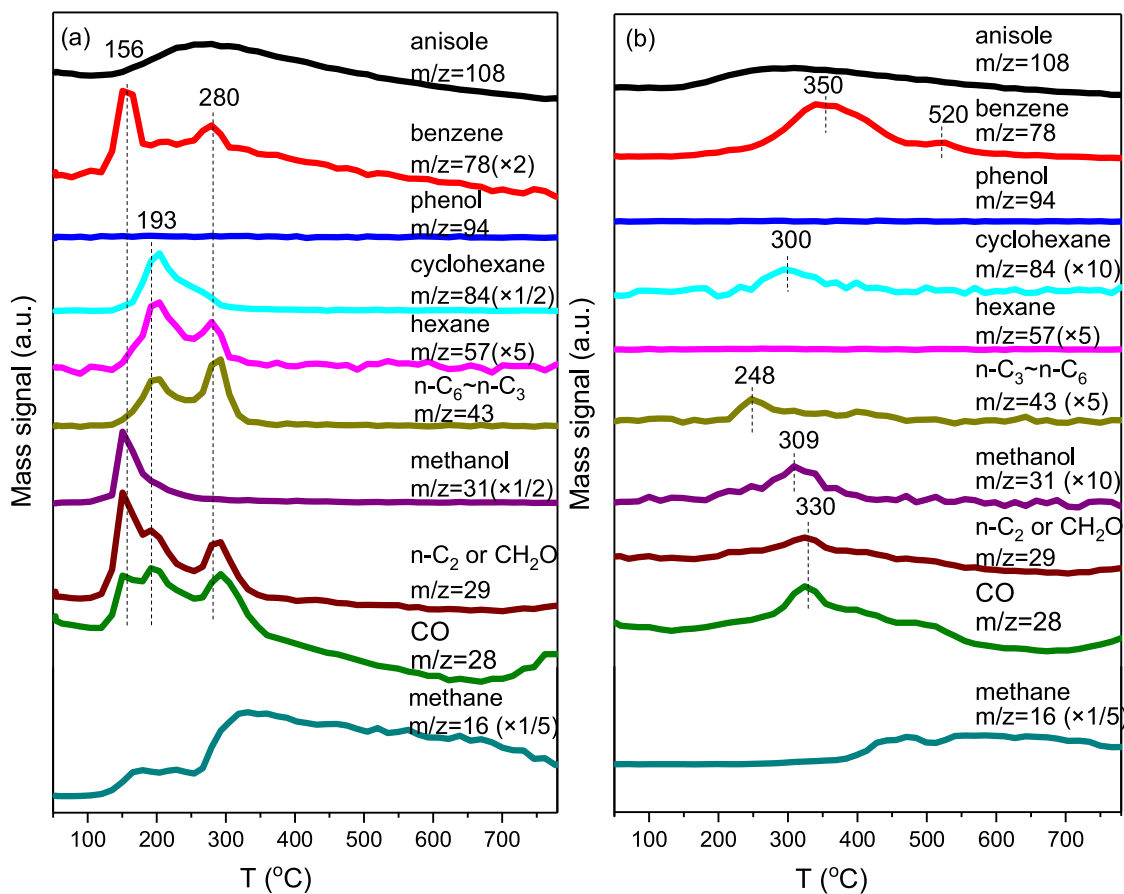


Fig. 9. Anisole-TPSR on (a) Ni/SiO₂ and (b) Ni₃Ga/SiO₂ purged with He at 550 °C. (Benzene signal ($m/z = 78$), corrected by subtracting the signal contributed from anisole).

methanol, CH₂O and CO, attributed to the scission of the C_{Ar}—OCH₃ group, the dehydrogenation of methanol and the decompose of CH₂O, respectively. Cyclohexane and n-C₂~n-C₆ alkanes were produced with the distinct peaks at ~180 °C. Similar to the case of the catalyst purged with He, a large amount of benzene was produced with a broad peak centered at 350 °C, accompanying with CH₂O and CO. There were no other peaks apart from a small peak ($m/z = 43$) at ~390 °C. In other words, the generated benzene was immediately desorbed from the catalyst surface and was difficultly further hydrogenated. Thus, we consider that the scission of the C_{Ar}—OCH₃ group to benzene was reaction limited at 350 °C. Here, it is surprising that the benzene hydrogenation followed by C—C bond hydrogenolysis took place below 250 °C but did not occur at higher temperature. In addition, methane was mainly detected at above 350 °C, indicating that high temperature is conducive to the O—CH₃ bond cleavage. This is also reflected by the influence of reaction temperature on the performance of Ni₃Ga/SiO₂ (Fig. S6). As shown in Fig. S6, with increasing temperature from 300 to 380 °C, the anisole conversion reached maximum (~74%) at 340~360 °C because the HDO of anisole is exothermic. The selectivity to benzene gradually decreased from 89% to 73%, accompanying the increase in the selectivity to phenol from 1.4% to 11%. Meanwhile, the n_{CH4}/n_{Anisole} molar ratio increased from 0.15 to 0.32 and the n_{CO}/n_{Anisole} molar ratio tended to decrease from 0.85 to 0.76.

3.4. Discussion

Herein, metallic Ni, Ni-Ga alloy with Ni/Ga atomic ratio of 6 and Ni₃Ga IMC formed in Ni/SiO₂, Ni₆Ga/SiO₂ and Ni₃Ga/SiO₂ (Fig. 2), respectively. In the Ni-Ga alloy and Ni₃Ga IMC, the continuous Ni atoms are isolated to form smaller Ni ensembles, giving rise to lower H₂

uptakes of Ni_xGa/SiO₂ than that of Ni/SiO₂ (Table 1). Moreover, there was a charge transfer from Ga to Ni (Fig. 3), leading to an increased electron density of the Ni atoms in Ni-Ga alloy and Ni₃Ga IMC. Reports have indicated that an alloy is a mixture and has a random atomic order, while an IMC is a single phase and has a long-range homogeneity [29,30]. As indicated by the XAFS characterization [26], the Ni atom is located at the face-centered position in the fcc Ni₃Ga IMC, and Ni—Ni and Ni—Ga bond lengths are equal (2.53 Å). The Ni—Ni bond length in Ni₃Ga IMCs is larger than that (2.49 Å) in metallic Ni [26]. In contrast to the homogeneity of Ga in Ni₃Ga IMCs, the Ga atoms random incorporate in the Ni lattice in Ni-Ga alloy of Ni₆Ga/SiO₂. Even though, the larger Ga atom make the Ni lattice expand and so the Ni—Ni bond length increase. Therefore, it is reasonably speculated that the Ni—Ni bond length increases in the order in Ni/SiO₂, Ni₆Ga/SiO₂ and Ni₃Ga/SiO₂, and the number of Ga atom bonded to Ni atom in Ni₃Ga IMCs is larger than that in Ni-Ga alloy with Ni/Ga atomic ratio of 6. In addition, the presence of Ga also increased the catalyst acidity as shown by NH₃-TPD (Fig. 4) and resulted in a great of spilt-over hydrogen on Ni_xGa/SiO₂ as shown by H₂-TPD (Fig. 5). The modification of Ga on the Ni/SiO₂ structure significantly influence the catalyst performance for HDO.

3.4.1. Catalyst activity

As shown in Fig. 6(A), on a whole, Ni_xGa/SiO₂ were more active than Ni/SiO₂ although they possessed lower H₂ uptake. We speculate that there is a synergism between the close proximal Ni and Ga atoms in Ni-Ga alloy and Ni₃Ga IMC. To verify this, a physical mixture of Ni/SiO₂ and Ga/SiO₂ particles was tested. For comparison, Ga/SiO₂ was also evaluated. As shown in Table 2, Ga/SiO₂ mainly gave phenol and cresol. This means that the hydrogen species (e.g., Ga-H and dihydrides) and acid sites on Ga/SiO₂ could catalyze the O—CH₃ bond

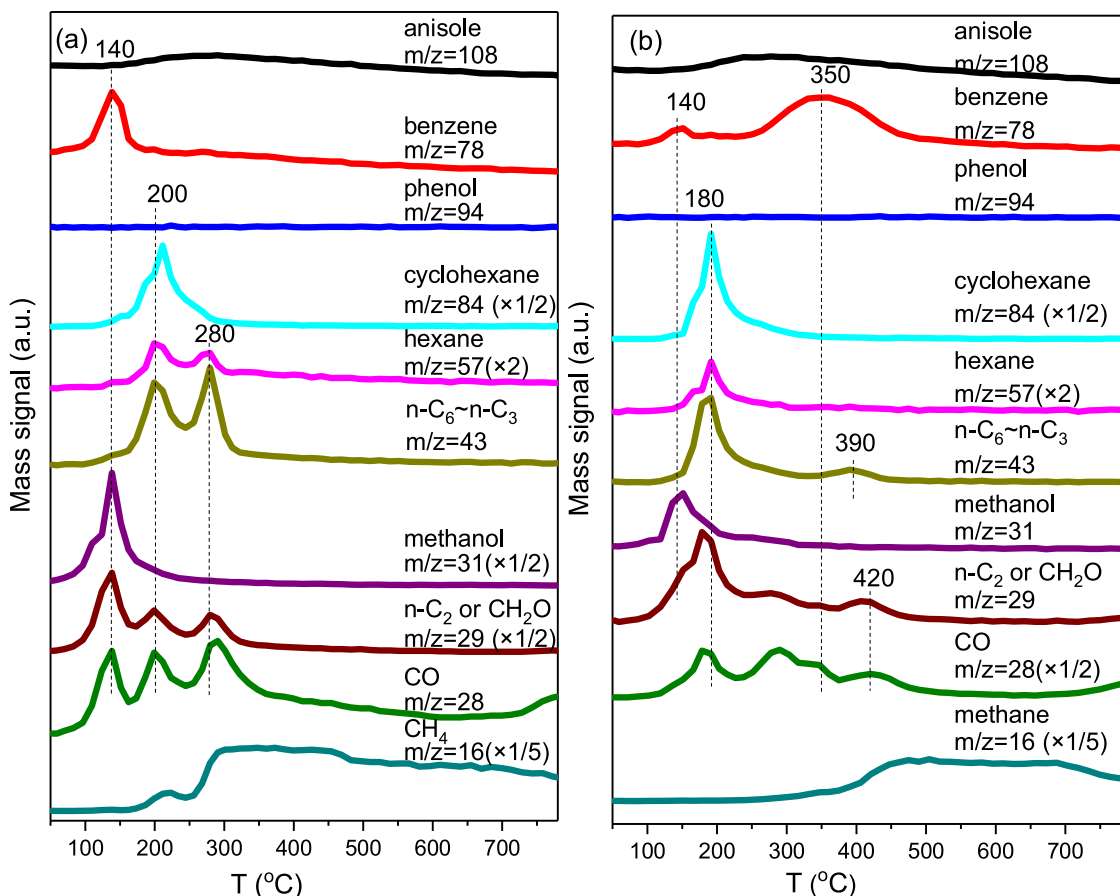


Fig. 10. Anisole-TPSR on (a) Ni/SiO₂ and (b) Ni₃Ga/SiO₂ without purge with He at 550 °C. (Benzene signal (*m/z* = 78), corrected by subtracting the signal contributed from anisole).

hydrogenolysis and the methyl transfer, respectively. Surprisingly, the conversion (13.2%) on the physical mixture was even lower than that (23.2%) on Ni/SiO₂ itself. We speculate that phenol produced on Ga/SiO₂ caused the carbon deposition [46], which covered the active sites and made the catalyst activity decrease. Based on the carbon deposit amounts measured by the TG method (detail in Fig. S7 in Supplementary information), the carbon deposition rates were estimated as 16.1, 7.0, 5.8 and 6.0 mg/(g·h) on Ga/SiO₂, Ni/SiO₂, Ni₆Ga/SiO₂ and Ni₃Ga/SiO₂, respectively. Clearly, Ga/SiO₂ gave the highest carbon deposition rate, followed by Ni/SiO₂. Additionally, according to the TG results, we consider that there were polymers produced during the reaction. The polymers were not detected by GC and so the total selectivity to the detected products were lower than 100% (Table 2). Particularly, the lower that the selectivity to phenol and cresol was, the more the total selectivity to the detected products was close to 100% (Table 2). This

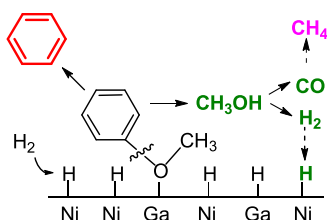
also indicates that phenol is apt to polymerize, consistent with the literatures [45,46]. A dual-layer Ni/Ga catalyst system was also evaluated, giving rise to higher conversion (29.5%) than that on Ni/SiO₂, very close to the sum of the conversions on separate Ni/SiO₂ and Ga/SiO₂. This further confirm that the lower conversion on the physically mixed Ni/SiO₂ and Ga/SiO₂ catalyst is due to the carbon deposition. Based on the above results, we suggest that the close proximity between Ni and Ga atoms, in alloy and IMC but not in the physical mixture of Ni/SiO₂ and Ga/SiO₂ particles, is essential to the synergism for the conversion of anisole. Given more homogeneity of Ga and more Ni–Ga bonds in Ni₃Ga, the synergistic effect between Ni was more effective on Ni₃Ga/SiO₂ than on Ni₆Ga/SiO₂. Thus, in the concerned catalysts, Ni₃Ga/SiO₂ showed the highest activity, reflected by the highest anisole conversion at same reaction condition (Fig. 6(A)) and the highest TOF (Table 1). As to the synergism, we speculate that the oxygen in anisole

Table 2

Anisole conversion and product distribution on Ni/SiO₂, Ga/SiO₂, Ni₆Ga/SiO₂, Ni₃Ga/SiO₂ and physical mixture of Ni/SiO₂ and Ga/SiO₂.

Catalyst	Conversion (%)	Selectivity (%)					<i>n</i> _{CO} / <i>n</i> _{Δanisole} molar ratio	<i>n</i> _{CH₄} / <i>n</i> _{Δanisole} molar ratio
		Benzene	Cyclohexane	Hexane	Phenol	Cresol		
Ni/SiO ₂ ^a	23.2	70.2	1.25	0.14	8.22	1.29	0.11	0.90
Ga/SiO ₂ ^b	5.18	0.58	0.14	0.02	54.9	29.4	0.00	0.00
Ni + Ga ^c	12.8	25.4	1.86	0.17	30.0	14.8	0.12	0.50
Ni/Ga ^d	29.5	55.6	1.09	0.08	23.4	6.75	0.12	0.82
Ni ₆ Ga/SiO ₂ ^e	24.1	85.4	4.03	0.13	4.02	1.13	0.63	0.17
Ni ₃ Ga/SiO ₂ ^f	27.6	92.6	3.22	0.10	2.55	0.93	0.69	0.02

^{a,b,e,f} anisole WHSV of 4 h⁻¹. ^c uniformly physical mixture of Ni/SiO₂ and Ga/SiO₂ particles with the equal mass. ^d a dual-layer catalyst system (Ni/SiO₂ particles place on Ga/SiO₂ ones with the equal mass). ^{a,c,d} Ni/SiO₂ mass was equal, and anisole WHSV of 4 h⁻¹ based on Ni/SiO₂. Reaction condition: 300 °C, 0.1 MPa, H₂/anisole molar ratio of 25.



Scheme 2. Possible reaction mechanism in HDO of anisole on $\text{Ni}_x\text{Ga}/\text{SiO}_2$. Steps connected by dashed lines are minor reaction pathways.

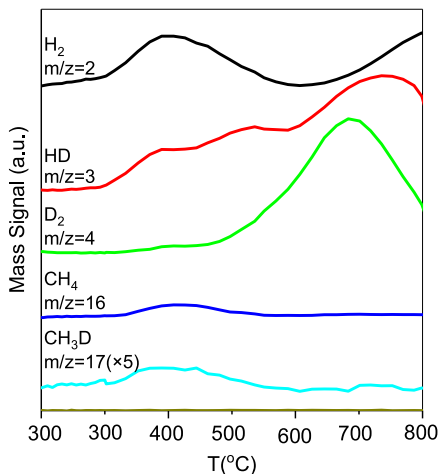


Fig. 11. Isotope tracing experiment on $\text{Ni}_3\text{Ga}/\text{SiO}_2$.

preferentially adsorb on Ga atom, and the activated C–O bond was attacked by the H species on Ni atoms and then converted (**Scheme 2**). This is also beneficial to the DDO pathway. The detail is further discussed in the following text.

In addition, the spilt-over hydrogen species on $\text{Ni}_x\text{Ga}/\text{SiO}_2$ may also contribute to the conversion of anisole. To explore this, an isotope tracing experiment was performed as described in Section 2.2. As shown in **Fig. 11**, H_2 and CH_4 should derive from the dehydrogenation of anisole and the cleavage of O– CH_3 bond [10], respectively. HD, monitored up to 800 °C, was derived from the combination of H and spilt-over D. A large peak due to D_2 desorption is observed at ~687 °C. Specially, CH_3D was synchronously produced with CH_4 with the peak centered at ~405 °C, indicating that a small amount of spilt-over D species participated in the cleavage of O– CH_3 bond. Given the H_2 -TPD results, we speculate that the spilt-over hydrogen species, located at the interface between the Ni_3Ga particle and support (corresponding to the H_2 desorption peak at ~416 °C in **Fig. 5(c)**, also facilitate the conversion of anisole.

3.4.2. Deoxygenation mechanism

Here, benzene was the main product on Ni/SiO_2 and $\text{Ni}_x\text{Ga}/\text{SiO}_2$. As shown in **Scheme 1**, benzene can be generated from the cleavage of $\text{C}_{\text{Ar}}\text{—OCH}_3$ bond in anisole and $\text{C}_{\text{Ar}}\text{—OH}$ bond in phenol. Phenol and $\text{CH}_3\text{OH}/\text{CO}$, generated on Ni/SiO_2 and $\text{Ni}_x\text{Ga}/\text{SiO}_2$, indicating that cleavage of both $\text{C}_{\text{Ar}}\text{—OCH}_3$ and O– CH_3 bonds took place.

From the product distribution in the HDO of anisole (**Fig. 6**) as well as the anisole-TPD and TPSR (**Figs. 8–10**) on Ni/SiO_2 and $\text{Ni}_x\text{Ga}/\text{SiO}_2$, it can be found that the cleavage of C–H and C–O bonds of adsorbed anisole was more easily on Ni/SiO_2 than on $\text{Ni}_3\text{Ni}/\text{SiO}_2$, while the O– CH_3 and $\text{C}_{\text{Ar}}\text{—OCH}_3$ bonds were preferentially cleaved on Ni/SiO_2 and $\text{Ni}_x\text{Ga}/\text{SiO}_2$, respectively. Also, the adsorption of benzene may be weaker on $\text{Ni}_3\text{Ga}/\text{SiO}_2$ than Ni/SiO_2 , and so the hydrogenation of benzene was suppressed on $\text{Ni}_3\text{Ga}/\text{SiO}_2$. This is consistent with the performance of $\text{Ni}_3\text{Ga}/\text{SiO}_2$ and Ni/SiO_2 in the hydrogenation of benzene (**Fig. S4**), contributing to higher selectivity to benzene on $\text{Ni}_3\text{Ga}/\text{SiO}_2$.

SiO_2 in the DHO of anisole.

To further present more preferential cleavage of $\text{C}_{\text{Ar}}\text{—O}$ bond on $\text{Ni}_3\text{Ga}/\text{SiO}_2$, the HDO of m-cresol was also selected to evaluate the performance of $\text{Ni}_3\text{Ga}/\text{SiO}_2$ and Ni/SiO_2 (**Table S2**). $\text{Ni}_3\text{Ga}/\text{SiO}_2$ gave both higher conversion (30.4%) and selectivity to toluene (48.2%) compared with Ni/SiO_2 (26.2% and 27.9%). Contrarily, Ni/SiO_2 had very higher selectivity to benzene (3.2%) and phenol (15.9%) than $\text{Ni}_3\text{Ga}/\text{SiO}_2$ (0.6% and 0.2%). Also, the selectivity to methane reached 14.8% on Ni/SiO_2 , methane was scarcely detected on $\text{Ni}_3\text{Ga}/\text{SiO}_2$. Thus, compared with Ni/SiO_2 , $\text{Ni}_3\text{Ga}/\text{SiO}_2$ was more preferential to cleave the $\text{C}_{\text{Ar}}\text{—O}$ bond while less active for the cleavage of C–C bond (including $\text{C}_{\text{Ar}}\text{—C}$).

As to more preferential cleavage of $\text{C}_{\text{Ar}}\text{—O}$ bond on Ni–Ga alloy and Ni_3Ga IMC, we suggest a synergistic effect between proximal Ni and Ga as shown in **Scheme 2**. On Ni–Ga alloy and Ni_3Ga IMC, oxygen in anisole might be apt to adsorb on Ga site because Ga possessed a small amount of positive charge as indicated by XPS results and Ga has stronger affinity to O than Ni speculated from H_2 -TPR. Consequently, the $\text{C}_{\text{Ar}}\text{—O}$ bond was easily activated and then attracted by the H species on the Ni site as well as spilt-over hydrogen at the interface between the alloy and IMC particles and support, subsequently resulting in the cleavage of $\text{C}_{\text{Ar}}\text{—O}$ bond to yield benzene. This is also verified by the result that the physical mixture of Ga/SiO_2 and Ni/SiO_2 particles gave lower selectivity to benzene and higher selectivities to phenol and cresol than Ni/SiO_2 itself (**Table 2**). The distance between Ni and Ga in the physical mixture was too long to make the synergistic effect. Additionally, Ga/SiO_2 dominantly gave phenol and cresol (**Table 2**), which is attributed to the cleavage of O– CH_3 bond. However, the H species on Ga/SiO_2 were difficult to break the $\text{C}_{\text{Ar}}\text{—O}$ bond to produce benzene. By contrast, the Ni and Ga atoms in alloy and IMC are very proximate, favoring their synergism. Moreover, in compared with those for $\text{Ni}_6\text{Ga}/\text{SiO}_2$, more homogeneity of Ga and more Ni–Ga bonds in Ni_3Ga for $\text{Ni}_3\text{Ga}/\text{SiO}_2$ are more beneficial to the synergism and DDO pathway to produce benzene. Also, the charge transfer from Ga to Ni led to high electron density of Ni atom in Ni–Ga alloy and IMC, which is not favorable for the adsorption of electron-rich benzene ring on the Ni atoms. The synergistic effect for HDO has also been found for the Pt–Zn [10], Ni–Re [9] and Pd–Fe [19] and Pt–Re [47] bimetallic are oxophilic sites on the supports [48]. Here, it is worth highlighting that H_2 produced from the decomposition of methanol on $\text{Ni}_x\text{Ga}/\text{SiO}_2$ may also adsorb on the catalyst and participate in the reaction (**Scheme 2**).

3.4.3. Benzene hydrogenation, C–C bond hydrogenolysis and methanation

Compared with Ni/SiO_2 , $\text{Ni}_3\text{Ga}/\text{SiO}_2$ were lower active for benzene hydrogenation, C–C bond hydrogenolysis and CO methanation due to the formation of Ni–Ga alloy and Ni_3Ga IMC (**Fig. S4** and **Fig. 7**). This is favorable for increasing the selectivity to benzene and inhibiting the CH_4 formation on $\text{Ni}_x\text{Ga}/\text{SiO}_2$ in HDO of anisole. It has been reported that the large Ni ensembles favor the benzene hydrogenation and C–C bond hydrogenolysis [49]. And the co-adsorption of two adjacent atoms is required to facilitate C–C bond cleavage [50]. In Ni–Ga alloy and Ni_3Ga IMC, the contiguous of Ni atoms are disrupted, leading to smaller Ni ensembles. This is unfavorable for the adsorption of benzene and cyclohexane as well as alkanes, and so the benzene hydrogenation and the of C–C bond hydrogdenolysis were suppressed. In addition, the charge transfer from Ga to Ni gives rise to the electron-enriched Ni species, which may also be unfavorable for adsorbing benzene because benzene is characterized by an electron-rich delocalized π system. It has been reported that benzene is bonded to the metal surface via π -bond involving an electron transfer from the aromatic ring to the unoccupied d-metal orbitals [51], and so benzene more preferentially adsorbs on electron-deficient metal site in comparison with the electron-enriched one [52]. It has been reported that the increase in electron density of Ni is beneficial to CO methanation [53], while smaller Ni ensembles are less active for the CO methanation [54]. Herein, a charge transfer from Ga to Ni increases the electron density of Ni, while the Ni ensembles

became smaller due to the isolation of Ga. The H₂ chemisorption results indicate that the isolated Ni atoms are less active for adsorbing/activating H₂, while the activating hydrogen is essential for CO methanation. That is, the geometric effect of Ga is unfavorable for the methanation on Ni-Ga alloy and IMC. Similar case was also found for Ni-In alloy and NiZn IMCs [20,55].

4. Conclusion

As indicated by XRD, a Ni-Ga alloy and Ni₃Ga IMC formed in Ni₆Ga/SiO₂ and Ni₃Ga/SiO₂, respectively. The contiguous Ni atoms are disrupted by Ga atoms, resulting in decreased surface Ni site density. XPS reveals a charge transfer from Ni to Ga in the alloy and IMC. Reactivity test, anisole-TPD and TPSR results indicate that the C_{Ar}—OCH₃ bond was more preferentially broken on Ni_xGa/SiO₂ than on Ni/SiO₂. At the same reaction condition, Ni_xGa/SiO₂ showed higher anisole conversion and selectivity to benzene and lower selectivity to phenol than Ni/SiO₂. This is attributed to the synergism between Ni and Ga and is also related to the spilt-over H species. Also, benzene hydrogenation and C—C bond hydrogenolysis were suppressed on Ni_xGa/SiO₂. It is highlighted that methanol, produced from the C_{Ar}—OCH₃ bond cleavage, decomposed to CO and H₂ on Ni_xGa/SiO₂, i.e., H₂ could be generated from anisole itself. However, methanol was dominantly converted to methane on Ni/SiO₂. In short, Ni_xGa/SiO₂ (especially Ni₃Ga/SiO₂) gave higher benzene yield and remarkably reduced H₂ consumption in comparison with Ni/SiO₂, which is mainly due to the geometric and electronic effects of Ga.

Acknowledgement

The authors gratefully acknowledge support from the National Natural Science Foundation of China (No. 21576193 and 21176177).

Appendix A. Supplementary data

Supplementary material related to this article can be found, in the online version, at doi:<https://doi.org/10.1016/j.apcatb.2019.02.073>.

References

- [1] H. Wang, J. Male, Y. Wang, ACS Catal. 3 (2013) 1047–1070.
- [2] M. Saidi, F. Samimi, D. Karimipourfard, T. Nimmanwudipong, B.C. Gates, M.R. Rahimpour, Energy Environ. Sci. 7 (2014) 103–129.
- [3] P.M. Mortensen, J.-D. Grunwaldt, P.A. Jensen, K.G. Knudsen, A.D. Jensen, Appl. Catal. A: Gen. 407 (2011) 1–19.
- [4] A. Demirbas, Energy Convers. Manag. 42 (2001) 1357–1378.
- [5] L. Nie, P.M. de Souza, F.B. Noronha, W. An, T. Sooknoi, D.E. Resasco, J. Mol. Catal. A: Chem. 388–389 (2014) 47–55.
- [6] A. Ausavasukhi, T. Sooknoi, D.E. Resasco, J. Catal. 268 (2009) 68–78.
- [7] Y. Romero, F. Richard, S. Brunet, Appl. Catal. B: Environ. 98 (2010) 213–223.
- [8] R.C. Nelson, B. Baek, P. Ruiz, B. Goundie, A. Brooks, M.C. Wheeler, B.G. Frederick, L.C. Grabow, R.N. Austin, ACS Catal. 5 (2015) 6509–6523.
- [9] F. Yang, D. Liu, H. Wang, X. Liu, J. Han, Q. Ge, X. Zhu, J. Catal. 349 (2017) 84–97.
- [10] D. Shi, L. Arroyo-Ramírez, J.M. Vohs, J. Catal. 340 (2016) 219–226.
- [11] C.A. Teles, P.M. de Souza, R.C. Rabelo-Neto, M.B. Griffin, C. Mukarakate, K.A. Orton, D.E. Resasco, F.B. Noronha, Appl. Catal. B: Environ. 238 (2018) 38–50.
- [12] R.N. Olcese, M. Bettahar, D. Petitjean, B. Malaman, F. Giovanella, A. Dufour, Appl. Catal. B 115–116 (2012) 63–73.
- [13] S.A. Khromova, A.A. Smirnov, O.A. Bulavchenko, A.A. Saraev, V.V. Kaichev, S.I. Reshetnikov, V.A. Yakovlev, Appl. Catal. A: Gen. 470 (2014) 261–270.
- [14] S. Wu, Po. Lai, Y. Lin, H. Wan, H. Lee, Y. Chang, ACS Sustainable Chem. Eng. 1 (2013) 349–358.
- [15] V.O.O. Goncalves, P.M. de Souza, T. Cabioc'h, V.T. da Silva, F.B. Noronha, F. Richarda, Appl. Catal. B: Environ. 219 (2017) 619–628.
- [16] E. Ochoa, D. Torres, R. Moreira, J.L. Pinilla, I. Suelves, Appl. Catal. B: Environ. 239 (2018) 463–474.
- [17] G.A. Mills, F.W. Steffgen, Catal. Rev. 8 (1974) 159–210.
- [18] X. Liu, W. An, C.H. Turner, D.E. Resasco, J. Catal. 359 (2018) 272–286.
- [19] J. Sun, A.M. Karim, H. Zhang, L. Kovarik, X.S. Li, A.J. Hensley, J. McEwen, Y. Wang, J. Catal. 306 (2013) 47–57.
- [20] X. Wang, J. Chen, Chin. J. Catal. 38 (2017) 1818–1830.
- [21] A. Bhan, W.N. Delgass, Catal. Rev. 50 (2008) 19–151.
- [22] A. Ausavasukhi, Y. Huang, A.T. To, T. Sooknoi, D.E. Resasco, J. Catal. 290 (2012) 90–100.
- [23] A.B. Getsoian, U. Das, J. Camacho-Bunquin, G. Zhang, J.R. Gallagher, B. Hu, S. Cheah, J.A. Schaidle, D.A. Ruddy, J.E. Hensley, T.R. Krause, L.A. Curtiss, J.T. Miller, A.S. Hock, Catal. Sci. Technol. 6 (2016) 6339–6353.
- [24] L. Wang, F. Li, Y. Chen, J. Chen, J. Energy Chem. 29 (2019) 40–49.
- [25] Y. Liu, X. Liu, Q. Feng, D. He, L. Zhang, C. Lian, R. Shen, G. Zhao, Y. Ji, D. Wang, G. Zhou, Y. Li, Adv. Mater. 28 (2016) 4747–4754.
- [26] C. Li, Y. Chen, S. Zhang, J. Zhou, F. Wang, S. He, M. Wei, D.G. Evans, X. Duan, ChemCatChem 6 (2014) 824–831.
- [27] E. Heracleous, A.A. Lemonidou, J. Catal. 270 (2010) 67–75.
- [28] K. Li, R. Wang, J. Chen, Energy Fuels 25 (2011) 854–863.
- [29] M. Armbrüster, R. Schlögl, Y. Grin, Sci. Technol. Adv. Mater. 15 (2014) 034803.
- [30] J. Osswald, R. Giedigkeit, R.E. Jentoft, M. Armbrüster, F. Girgsdies, K. Kovnir, T. Ressler, Y. Grin, R. Schlögl, J. Catal. 258 (2008) 210–218.
- [31] A. Fakhri, S. Behrouz, M. Asif, I. Tyagi, S. Agarwal, V.K. Gupta, J. Mol. Liq. 213 (2016) 326–331.
- [32] F. Scharmann, G. Cherkashinin, V. Breternitz, C. Knedlik, G. Hartung, T. Weber, J.A. Schaefer, Surf. Interface Anal. 36 (2004) 981–985.
- [33] V.V. Kaichev, A.Y. Gladky, I.P. Prosvirin, A.A. Saraev, M. Hävecker, A. Knop-Gericke, R. Schlögl, V.I. Bukhtiyarov, Surf. Sci. 609 (2013) 113–118.
- [34] A.M. Venezia, R. Bertoncello, G. Deganello, Surf. Interface Anal. 23 (1995) 239–241.
- [35] M. Grabau, H.P. Steinrück, C. Papp, Surf. Sci. 677 (2018) 254–257.
- [36] Y. Fang, X. Su, X. Bai, W. Wu, G. Wang, L. Xiao, A. Yu, J. Energy. Chem. 26 (2017) 768–775.
- [37] G. Connell, J.A. Dumesic, J. Catal. 105 (1987) 285–298.
- [38] K. Fang, J. Ren, Y. Sun, J. Mol. Catal. A: Chem. 229 (2005) 51–58.
- [39] J.K. Kim, J.K. Lee, K.H. Kang, J.C. Song, I.K. Song, Appl. Catal. A: Gen. 498 (2015) 142–149.
- [40] S.E. Collins, M.A. Baltanás, J.L.G. Pierro, A.L. Bonivardi, J. Catal. 211 (2002) 252–264.
- [41] A.G. Boudjahem, S. Monteverdi, M. Mercy, D. Ghanbaja, M.M. Bettahar, Catal. Lett. 84 (2002) 115–122.
- [42] J.A. Cecilia, I. Jiménez-Morales, A. Infantes-Molina, E. Rodríguez-Castellón, A. Jiménez-López, J. Mol. Catal. A: Chem. 368–369 (2013) 78–87.
- [43] J.T. Miller, B.L. Meyers, F.S. Modica, G.S. Lane, D.C. Koningsberger, J. Catal. 143 (1993) 395–408.
- [44] W.C. Conner, J.L. Falconer, Chem. Rev. 95 (1995) 759–788.
- [45] X. Lan, E.J.M. Hensen, T. Weber, Appl. Catal. A: Gen. 550 (2018) 57–66.
- [46] A. Popov, E. Kondratieva, J.M. Goupil, L. Mariey, P. Bazin, J. Gilson, A. Travert, F. Maugé, J. Phys. Chem. C 114 (2010) 15661–15670.
- [47] Z. Wei, X. Zhu, X. Liu, H. Xu, X. Li, Y. Hou, Y. Liu, Chin. J. Chem. Eng. (2018), <https://doi.org/10.1016/j.cjche.2018.04.022> In press.
- [48] K.A. Resende, A.H. Braga, F.B. Noronha, C.E. Hori, Appl. Catal. B: Environ. 245 (2019) 100–113.
- [49] J.H. Sinfelt, Acc. Chem. Res. 10 (1977) 15–20.
- [50] D.D. Hibbitts, D.W. Flaherty, E. Iglesia, ACS Catal. 6 (2015) 469–482.
- [51] A. Stanislaus, B.H. Cooper, Catal. Rev.-Sci. Eng. 36 (1994) 75–123.
- [52] G. Zhou, H. Wang, J. Tian, Y. Pei, K. Fan, M. Qiao, B. Sun, B. Zong, ChemCatChem 10 (2018) 1184–1191.
- [53] Y. Okamoto, E. Matsunaga, T. Imanaka, S. Teranishi, J. Catal. 74 (1982) 183–187.
- [54] L. Gan, R. Tian, X. Yang, H. Lu, Y. Zhao, J. Phys. Chem. C 116 (2011) 745–752.
- [55] Z. Pan, R. Wang, J. Chen, Appl. Catal. B: Environ. 224 (2018) 88–100.